Orbital Angular Momentum Assisted Ground Penetrating Radars

Daniel Orfeo*[a], Wilson Ezequelle[a], Tian Xia[b], Dryver Huston*[a]
[a] Mechanical Engineering Department, University of Vermont, Burlington, VT USA 05405-0156;
[b] Electrical and Biomedical Engineering Department, University of Vermont, Burlington, VT USA 05405-0156

ABSTRACT

This paper explores using Orbital Angular Momentum (OAM) controlled electromagnetic waves for enhanced ground penetrating radar (GPR) imaging and detection. A macroscopic interpretation of OAM is propagating waves with vortex-shaped wave fronts. At the photon level OAM appears as a quantum degree of freedom with integer quanta of angular momentum added to each photon. This is in addition to Spin Angular Momentum (SAM). The use of OAM in GPR has at least two potential advantages. The vortex shape may enable better discernment of cylindrical versus non-cylindrical buried objects. At the quantum level entanglement of OAM with other quantum degrees of freedom may enable enhanced imaging, such as the ghost imaging of objects that produce weak signal returns. The results include experiments that demonstrate the generation and reception of EM waves with a circular pattern of antennas operating as phased arrays to produce vortex-shaped waves at frequencies and dimensions typical of conventional GPRs.
Keywords: electromagnetic vortex, orbital angular momentum, ground penetrating radar

1. INTRODUCTION

Ground penetrating radar (GPR) and wall penetrating radars operate by launching, receiving and analyzing electromagnetic (EM) waves that interact with subsurface features in dielectric structures, such as the earth, concrete structures and building walls. The primary interactions rely on the spatially varying dielectric properties of structural material to reflect, scatter and absorb electromagnetic waves. Each of these interactions depends on the interplay of wavelength, polarization, and the geometric distribution of dielectric parameters. An example appears in Figure 1 where the relative direction of linear polarization has a dramatic effect on the ability to resolve steel reinforcing bars in concrete. Strong reflections occur when the polarization of the $\vec{E}$ field aligns with the conductive path of the reinforcing bar as the antenna passes over in a transverse direction. The B-scans show the rebar reflections as hyperbolas due to the geometric nonlinearity of off-axis reflections.

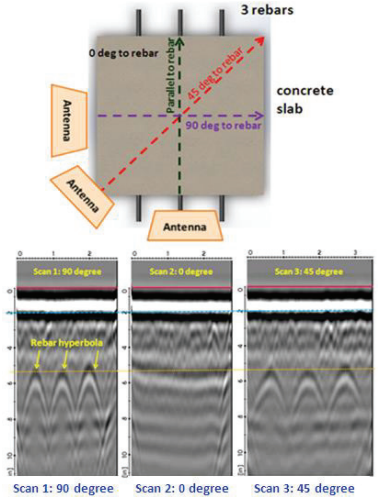

Figure 1. Effect of linear polarization direction on B-scans and the ability to detect steel reinforcing bars in concrete

*dryver.huston@uvm.edu; phone 1 802-656-1922;

The present state-of-the-art is that GPR is a mature technology that continues to improve in capabilities, yet still has significant performance limitations due to attenuation in lossy media, scattering in heterogeneous media, clutter and resolution of complicated geometries. The results in Figure 1 show that subsurface imaging performance can depend on geometric properties of the propagating field, such as polarization. Developments over the past two decades indicate that other controls over the geometry of the propagating waves are possible, including those with OAM.

Beams of EM fields with rotating kinematics degrees of freedom for control and use in sensing that extend beyond those available with conventional non-rotating fields. This is possible with both classical macroscopic and quantum effects. To date, most of the applications of rotating-field beams have occurred in the optical regime[1]. Desktop experiments presented in this paper confirm that it is possible to generate and sense vortex-shaped EM waves with phased antenna array methods. Possible future directions include application to GPR, ghost imaging, and exploitation of quantum effects for enhanced sensitivity.

2. MACROSCOPIC ROTATING ELECTROMAGNETIC BEAMS

Most penetrating radars use EM beams as the launched waves. In this context EM beams are collections of waves that travel in the same direction, centered on an axis. Figure 2 shows a generic beam propagating along the z-axis.

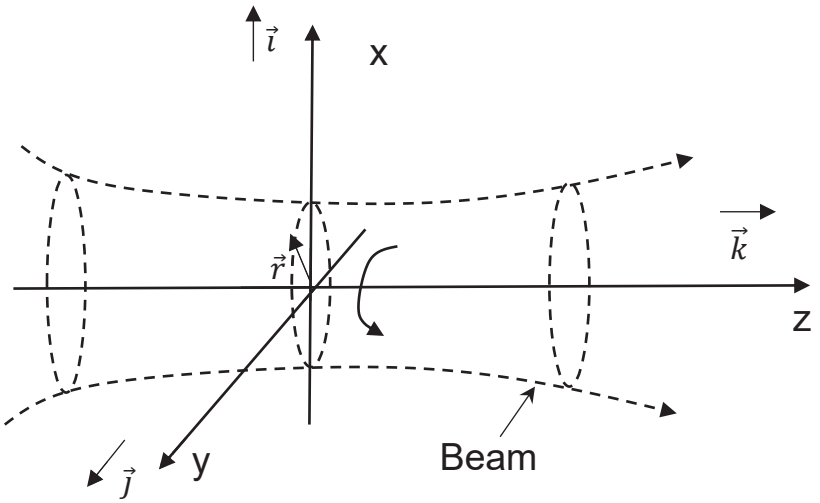

Figure 2. Electromagnetic beam centered on and propagating along z-axis with possible rotation component

In classical physics, the principal EM vector fields are the electric field $\vec{E}$, and the magnetic field, $\vec{B}$. Maxwell's equations describe propagating EM fields, including those in a beam[2].

$$\nabla \times \vec{\mathrm{B}} = \frac{1}{\mathrm{c}^2}\frac{\partial \vec{\mathrm{E}}}{\partial \mathrm{t}} \tag{1}$$

$$\nabla \times \vec{\mathrm{E}} = -\frac{\partial \vec{\mathrm{B}}}{\partial \mathrm{t}} \tag{2}$$

$$\nabla \cdot \vec{\mathrm{B}} = 0 \tag{3}$$

$$\nabla \cdot \vec{\mathrm{E}} = 0 \tag{4}$$

In a vacuum, or air at most wavelengths and power levels, ϵ_0 = 8.854 x 10^{-12} farad/m, $\mu_0 = 4\pi$ x 10^{-7} N/A^2 and c = 2.998 x 10^8 m/s. Combining the curl of (1) and (2) with (3) and (4) and using the identity for an arbitrary continuous vector field $\vec{A}$

$$\nabla\times\nabla\times\vec{\mathrm{A}}=\nabla\nabla\cdot\vec{\mathrm{A}}-\nabla^2\vec{\mathrm{A}} \tag{5}$$

leads to the vector wave equations and vector waves

$$\nabla^2\vec{\mathrm{E}}=\frac{1}{\mathrm{c}^2}\frac{\partial^2\vec{\mathrm{E}}}{\partial\mathrm{t}^2} \tag{6}$$

$$\nabla^2\vec{\mathrm{B}}=\frac{1}{\mathrm{c}^2}\frac{\partial^2\vec{\mathrm{B}}}{\partial\mathrm{t}^2} \tag{7}$$

c is the wave speed. The EM field propagates through space with linear momentum density $\vec{g}$ in terms of the Poynting vector $\vec{S}$ as

$$\vec{\mathrm{g}}=\epsilon_0\vec{\mathrm{E}}\times\vec{\mathrm{B}}=\epsilon_0\vec{\mathrm{S}} \tag{8}$$

The OAM density $\vec{\mathrm{L}}$ at a point with position $\vec{r}$ is with respect to a fixed reference point is the moment

$$\vec{\mathrm{L}}=\vec{\mathrm{r}}\times\vec{\mathrm{g}}=\epsilon_0\vec{\mathrm{r}}\times\left(\vec{\mathrm{E}}\times\vec{\mathrm{B}}\right)=\epsilon_0\vec{\mathrm{r}}\times\vec{\mathrm{S}} \tag{9}$$

In an isotropic medium with monochromatic fields, i.e. oscillating at a single frequency, $\vec{\mathrm{E}}\perp\vec{\mathrm{B}}$. Monochromatic plane waves propagating in the z-direction at a frequency ω and wavenumber $\mathrm{k}=\frac{\omega}{\mathrm{c}}$ have uniform properties in the x- and y-directions with electric and magnetic fields

$$\vec{\mathrm{E}}=\vec{\mathrm{E}}_0\mathrm{e}^{\mathrm{i}(\mathrm{kz}-\omega\mathrm{t})} \tag{10}$$

$$\vec{\mathrm{B}}=\vec{\mathrm{B}}_0\mathrm{e}^{\mathrm{i}(\mathrm{kz}-\omega\mathrm{t})} \tag{11}$$

with $\vec{\mathrm{E}}_0$ and $\vec{\mathrm{B}}_0$ constant vectors, possibly complex, and both in laying in the x-y plane perpendicular to the direction of propagation, z. Since the $\vec{\mathrm{E}}$ and $\vec{\mathrm{B}}$ fields are orthogonal, the cross-product and linear momentum point in the z-direction. The momentum density is homogeneous for a plane wave. Integration of the z-component of the OAM density in the x-y plane for plane waves then leads to zero angular momentum.

Scalar waves describe many properties of corresponding vector waves and provide a guide to approximate solutions, including descriptions of beams[3]. The scalar wave equation is

$$\nabla^2\psi=\frac{1}{\mathrm{c}^2}\frac{\partial^2\psi}{\partial\mathrm{t}^2} \tag{12}$$

Monochromatic scalar waves propagate at a constant frequency with a separable form

$$\psi(x,y,z,t)=\varphi(x,y,z)e^{i\omega t} \tag{13}$$

Substitution of the separable form into the wave equation leads to the spatial Helmholtz equation

$$\nabla^2\varphi + k^2\varphi = 0 \tag{14}$$

Solutions to the Helmholtz equation are the spatial envelopes of oscillating waves. Among the possible solutions are plane waves and beams.

Durnin[4] demonstrated the existence of a class of beams derived from the scalar wave equation with intensity distributions that do not change with propagation. Theses beams, known as diffraction-free or propagation-invariant, have the general form

$$\mathrm{E}(\mathrm{x},\mathrm{y},\mathrm{z}\geq 0,\mathrm{t}) = \exp[\mathrm{i}(\beta\mathrm{z}-\omega\mathrm{t})]\int_0^{2\pi}\mathrm{A}(\varphi)\exp[\mathrm{i}\alpha(\mathrm{x}\cos\varphi+\mathrm{y}\sin\varphi)]\mathrm{d}\varphi \tag{15}$$

with the constraint

$$\beta^2+\alpha^2 = \left(\frac{\omega}{\mathrm{c}}\right)^2 \tag{16}$$

A(φ) is an arbitrary complex integrable function. Direct substitution of the diffraction-free beam, (39), verifies that it is a solution to the Helmholtz equation. A simplification is to set A(φ) to a constant to creates a subset of solutions, known as Bessel beams, with field E_B,

$$\mathrm{E_B}(\mathrm{x},\mathrm{y},\mathrm{z}\geq 0,\mathrm{t}) = \exp[\mathrm{i}(\beta\mathrm{z}-\omega\mathrm{t})]\int_0^{2\pi}\exp[\mathrm{i}\alpha(\mathrm{x}\cos\varphi+\mathrm{y}\sin\varphi)]\mathrm{d}\varphi \tag{17}$$

Leading to cylindrical symmetry of intensity,

$$\mathrm{E_B}(\mathrm{x},\mathrm{y},\mathrm{z}\geq 0,\mathrm{t}) = \exp[\mathrm{i}(\beta\mathrm{z}-\omega\mathrm{t})]\mathrm{J}_0(\alpha\mathrm{R}) \tag{18}$$

J_0 is a Bessel function of the first kind of zero order. These beams, known as Bessel beams, have an invariant intensity distribution, I_B,

$$\mathrm{I_B} = \frac{1}{2}|\mathrm{J}_0(\alpha\mathrm{R})|^2 \tag{19}$$

If α= 0, then $J_0(\alpha R) = 1$, and the Bessel beam reverts to the special case of a plane wave. Like plane waves Bessel beams are physically unrealizable due to an infinite lateral extent and total energy. Bessel beams have a noteworthy self-healing property in that partial blockages and obstructions produce shadows that disappear with propagation distance due to a self-compensating diffraction.

Elongated monochromatic beams with relatively small gradients of shape with respect to the propagation axis permit approximating the Helmholtz equation with the paraxial wave equation. The approximation for a scalar wave propagating in the z-direction is to appear approximately as a plane wave where

$$\varphi(x,y,z) = A(x,y,z)e^{-ikz} \tag{20}$$

with A(x,y,z) varying slowly compared with the wavelength. This leads to the simple form of the paraxial wave equation

$$\frac{\partial^2 A}{\partial x^2} + \frac{\partial^2 A}{\partial y^2} - i2k\frac{\partial A}{\partial z} = 0 \tag{20}$$

It is of interest to note that (20) is in the form of a Schrödinger equation. The Gauss-LaGuerre (GL) modes are a set of solutions for beams. In cylindrical coordinates the GL modes $A_{GL}(r, \theta, z)$ are

$$A_{GL}(r, \theta, z) = \frac{C}{\left(1+\frac{z^2}{z_R^2}\right)^{\frac{1}{2}}}\left(\frac{r\sqrt{2}}{w(z)}\right)^{l} L_G^{l}\left(\frac{2r^2}{w^2(z)}\right) \times \exp\left(\frac{-r^2}{w^2(z)}\right)\exp\left(\frac{-ikr^2 z}{2\left(z^2+z_R^2\right)}\right)\exp(-il\theta) \times \exp\left(i(2p + l + 1)\operatorname{atan}\left(\frac{z}{z_R}\right)\right) \tag{21}$$

with z_R as the Raleigh range, w(z) as the beam radius, L_G^l as the associated Laguerre polynomial of order l and C is a constant[5]. The individual components of the $\vec{E}$ and $\vec{B}$ fields in propagating EM waves satisfy the Helmholtz equation, but are also collectively constrained by Maxwell's equations. For Gauss-Laguerre beams based on the assumption of transverse $\vec{E}$ fields, the $\vec{B}$ fields produce a non-transverse component, leading to a helix. Allen et al. showed that integrating the angular momentum density of these beams about the z-axis produces a non-zero angular momentum[6]. The ratio of angular momentum L to linear momentum P in terms of the wavelength λ is

$$\frac{L}{P} = \frac{l\lambda}{2\pi} \tag{22}$$

The introduction of Gauss-LaGuerre (GL) modes can produce EM beams with OAM. Each mode has a helical geometry, with the mode number corresponding to the number of intertwined helices[6]. The GL modes are mutually orthogonal. Cheng realized the production of GL modes in 97 GHz microwaves using waveplates with spiral patterns of holes[7]. Spiral phase plates can introduce vorticity into optical beams[8]. These plates enable the precise measurement of the phase distortion due to nanoscale textures on surfaces[9].

3. QUANTUM OAM EFFECTS

The quantum representation of propagating EM waves is with photons. The quantum representation of linear momentum is with an operator $\hat{p}$ acting on position q as an observable and the states as eigenvalues of the operator, where

$$\hat{p} = -ih\nabla \tag{23}$$

For a photon, the linear momentum states are discrete integer multiples of the Plank constant $h = 2\pi\hbar$ with $\hbar$ = 1.054 x 10^{-34} J-s/rad. Taking the moment ($\vec{r} \times \hat{p}$) of the linear momentum operator produces an angular momentum operator $\hat{l}$. The possible eigenvalue states of angular momentum form two sets of discrete values[10]. In both sets, the difference between states is integer multiples of $\hbar$. One set has multiples with the integers ...-2, -1, 0, 1, 2... The other set has half-integer multiples ...-3/2, -1/2, 1/2, 3/2... Isolated fermions, e.g. electrons, fall into the latter set with spin angular momentum states of -1/2 and 1/2. Based on arguments of symmetry and invariance of the associated relativistic tensors, photons are bosons

and fall into the former set with spin angular momentum states of -1 and 1[11]. In addition to spin, photons have orbital angular momentum state components of integers. It may remain an open question as to whether it is possible in general to measure SAM and OAM as separable field components[10,11].

Quantum-based radar systems hold the potential to provide superior sensing capabilities[12]. Several distinct approaches, most based on entanglement and some based on quantized OAM, have been proposed:

Quantum illumination for enhanced sensitivity – Uses entangled photons for enhanced photodetection[13,14,15]. The methods projects one set of photons onto the object under study and retains entangled complementary photons, i.e. ancilla, at the source. Photons reflected from the target combine with the entangled ancilla photons to produce an image, while rejecting unentangled photons. The result is enhanced sensitivity in presence of noise that is not possible with classical imaging systems.

Compressive sensing for quantum illumination – Compressive sensing is a technique that allows sensing of signals with sparse information content by undersampled measurements. Compressive sensing methods can be very effective in quantum illumination and imaging applications where using a dense of array of detectors is not practical[16].

Quantum interferometric sensing for enhanced depth of penetration – Allen (2008) patented a method for enhanced penetration and transmission of radar signals through lossy media with entangled photons[17]. The concept is to entangle groups of low-frequency, long-wavelength photons so that they interfere upon return to provide the effective spatial resolution of high frequency short wavelength photons, but with the lower attenuation rates of low-frequency photons. Experiments confirm the viability of these methods have been verified with experiments and can be further enhanced with adaptive optics[18].

Hyperentanglement – Elementary objects, such as photons, possess multiple quantum degrees of freedom. It is possible to entangle certain degrees of freedom while leaving others unentangled. This is known as hyperentanglement. An example is the quantized OAM of a photon. OAM degrees of freedom are distinct from polarization and wavelength. Hyperentanglement has the potential for significantly increasing the performance of sensors by enhancing resolution, signal-to-noise ratios and measurement time[19]. Entanglement and OAM entanglement distillation with Hong-Ou-Mandel interference may be able to improve the transmission of photons through atmospheric turbulence[20,21].

Frequency-domain or wavelength entanglement – The generation and detection of individual sets of photons in the time domain can be challenging, especially for microwave frequencies. Frequency domain entanglement is a potentially viable workaround. It uses larger numbers of photons and entangles them by frequency content. Physical methods of generation include nonlinear frequency combs and ring resonators, optomechanical resonators, and molecular magnets[22-28].

Metamaterial entanglement – It is possible to use metamaterials to entangle the spin and orbital angular momentum of photons[29]. The distinctive nature of photons and EM waves with different orbital angular momentum and vorticity allows for multiplexing multiple signals with the same frequency[30]. Custom lasers with integrated spiral waveplates can produce visible laser beams with specified vorticity[31].

Quantum Doppler sensing – It is possible to use quantum delay lines to implement quantum Doppler sensing for enhanced sensing in applications requiring low-level radiated emissions[32].

Ghost Imaging – Experiments in the optical domain using counting of photons with entangled OAM showed enhanced edge detection with phase differences that exceed classical correlations with violations of Bell's inequality[33].

4. ORBITAL ANGULAR MOMENTUM FOR PENETRATING RADARS

The control of OAM in penetrating radars opens up the possibility for multiple experiments to test the viability of improved performance. The configuration of the system appears in Figure 3. Numerical simulations show the potential for improve

azimuthal scanning with concentric array OAM radar systems[34]. OAM optical beams have the potential for robust transmission through turbulent air by adjusting beam vorticity parameters[35]. Of particular interest is whether OAM beams interact with shaped subsurface features, such as congested pipes or corners, in manners different than that of non-rotating beams. It is also of interest whether quantum radars using OAM hyperentanglement may offer better performance, such as increased sensitivity versus depth in lossy soils and increased subsurface Doppler sensitivity.

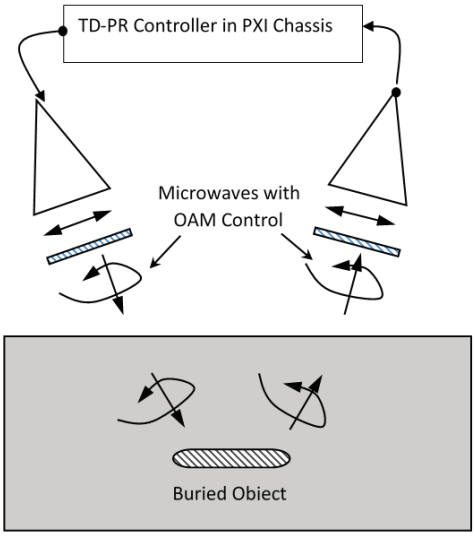

Figure 3. Bi-static OAM penetrating radar test configuration

5. PHASED-ARRAY ORBITAL ANGULAR MOMENTUM EXPERIMENTS

A set of experiments examined the viability of sending and receiving microwave beams containing controllable OAM at frequencies and dimensions comparable to those used in typical GPRs. Figure 4 shows a testbed. This is a phased-array system with four send and four receive linearly polarized antennas. The spatial configuration is that each set of four antennas uses a planar arrangement. Three of the antennas lie in an equilateral triangle and one is at the center. The polarization for all the antennas is linear and in the same direction. The system uses a modular PXIe microwave system (Keysight M9037A) for digital control of the input and output using 50 MHz baseband signals mixed up to microwave frequencies and back to the baseband with an intermediate frequency (IF) of 750 MHz.. Independent control is possible for each of the send channels.

The rationale for the antenna configuration is to use the three outer antennas (1, 2 and 3) to create a vortex through phase difference control and to use the center antenna (4) for an independent wave, possibly interfering with the other three in a ghost imaging application. The polarization of all eight antennas is aligned with the intent of reducing polarization effects. Figure 5 shows a typical received signal in the upconverted state with the 50 MHz baseband producing a beating effect on the carrier IF of 750 MHz. Time histories in the subsequent figures are downconverted to the baseband.

It is hypothesized that sending sinusoids at the same frequency, but with a 120 degrees phase offset out of channels 1, 2 and 3 will produce a vortex beam. Measuring this beam should produce sinusoids at receive channels 1, 2, and 3 with the same frequency and 120 degrees offset, along with a weak signal at the center receive antenna 4. The results shown in Figure 6 confirm this hypothesis with strong received signals in channels 1, 2 and 3 with 120 degrees offset and a weak signal at channel 4. A test to confirm the vortex shape involved sliding the receive frame laterally so that antenna 4 aligns with the perimeter of the outer send antenna pattern. The results shown in Figure 7 show that channel 4 is now strong. The next tests used the same setup as in Figures 4 and 6, but with an additional sinusoid at the same frequency driven out of the center channel 4. Figure 8 shows the addition of the center signal produces the same pattern in the outer channels 1, 2

and 3, but now with a stronger signal at the center channel 4. Sending sinusoids with different frequencies 40, 50 and 60 MHz out of channels 1, 2 and 3 produces mixed, somewhat incoherent, beating signals, Figure 9.

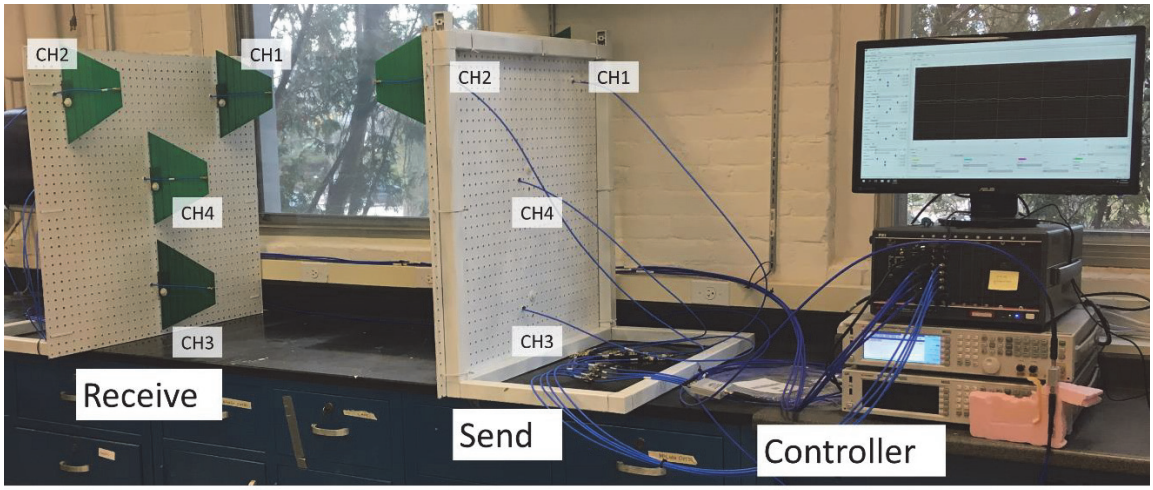

Figure 4. 4-channel send and 4-channel receive phased array microwave OAM testbed.

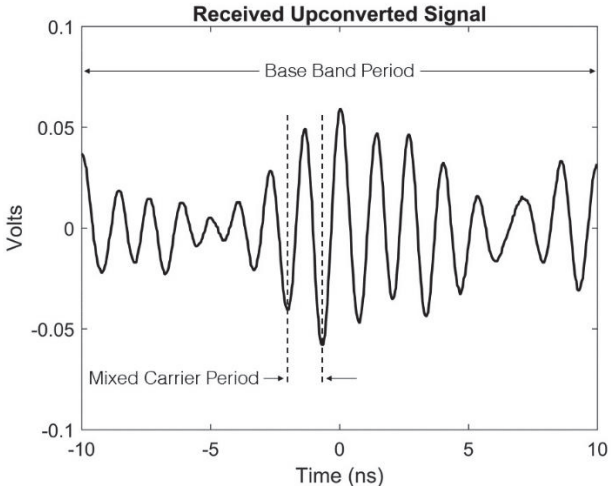

Figure 5. Typical mixed signal received at antenna containing both the baseband as a beating at 50 MHz and a faster IF band at 750 MHz

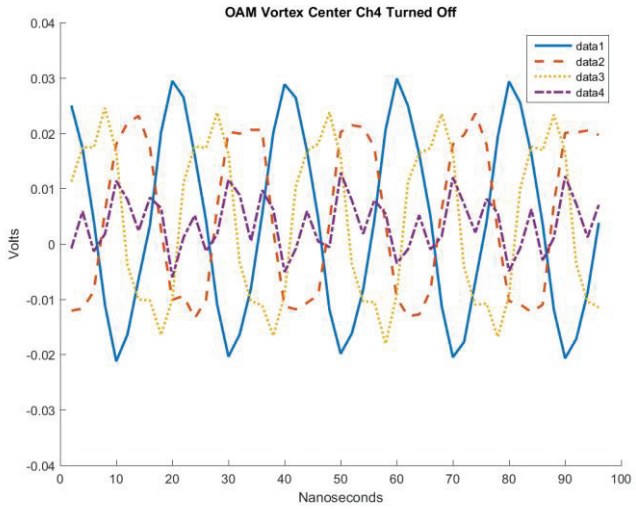

Figure 6. Received EM vortex with center send channel 4 off. Outer receive channels 1, 2 and 3 show 120 degree phasing and the center receive channel 4 has small amplitude.

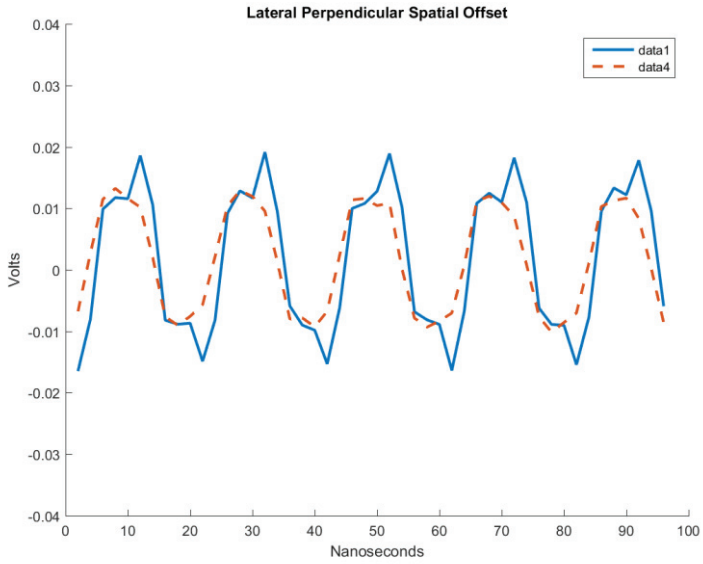

Figure 7. Lateral movement of receive array moves center receive channel 4 to vortex perimeter which aligns with outer receive channel 1

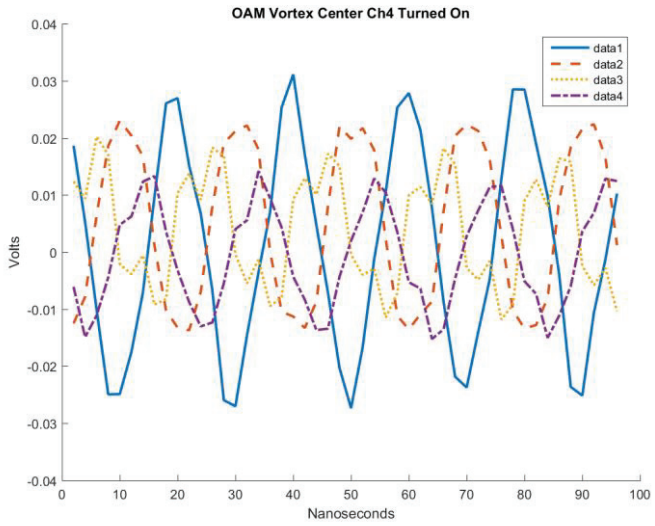

Figure 8. Received EM vortex with center send channel 4 off. Outer receive channels 1, 2 and 3 show 120-degree phasing and the center receive channel 4 has larger amplitude.

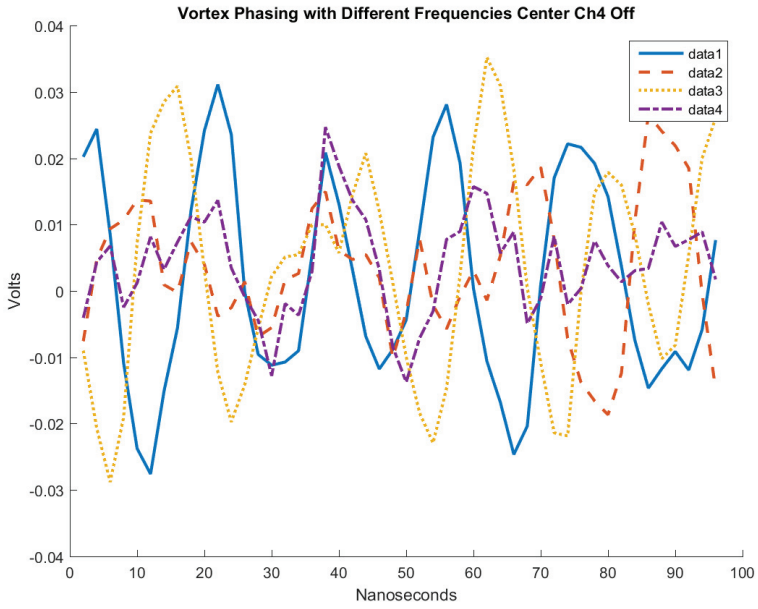

Figure 9. Sending of mixed frequencies with basebands of 40 MHz channel 1, 50 MHz channel 2 and 60 MHz channel 3 produce an incoherent beating signal at the receive antennas.

6. CONCLUSIONS

OAM is a degree of freedom in EM beams that has the potential for improving the performance of penetrating radars. Experiments demonstrate that is possible to generate beams containing OAM with frequencies and characteristic lengths comparable to those used in penetrating radars with phased array techniques.

ACKNOWLEDGEMENTS

This work has been supported by the Defense University Research Instrumentation Program (DURIP) U.S. Army contract no. W911NF1810193, U.S. Army contract W909MY-17-C-0020 with White River Technologies, U.S. National Science Foundation grants 1647095 and 1640687, the UVM Office or the Vice President for Research, and by the Vermont Space Grant Consortium under NASA Cooperative Agreement NNX15AP86H.

REFERENCES

[1] Yao, A. M., and Padgett, M.J., "Orbital Angular Momentum: Origins, Behavior and Applications" Advances in Optics and Photonics 3, 2, 161-204 (2011).

[2] Wangsness, R. K., [Electromagnetic Fields, 2nd ed.], Wiley, New York, 359-361 (1986).

[3] Saleh, B. E., Teich, M. E., [Fundamental of Photonics], Wiley, New York, 45-51 (1991).

[4] Durnin, J., "Exact Solutions for Nondiffracting Beams. I. The Scalar Theory" J Opt Soc Am, 4, 4, 651- 654 (1987).

[5] Allen, L., Beijersbergen, M.W., Spreeuw, R.J., and Woerdman, J.P., "Orbital Angular Momentum of Light and the Transformation of Laguerre-Gaussian Laser Modes" Phys. Rev. A 45, 8185 (1992).

[6] Yuan, T., Wang, H., Cheng, Y., and Qin, Y. "Electromagnetic Vortex-Based Radar Imaging Using a Single Receiving Antenna: Theory and Experimental Results" Sensors 2017, 17(3), 630 (2017).

[7] Cheng, L., Hong, W., and Hao, Z. C., "Generation of Electromagnetic Waves with Arbitrary Orbital Angular Momentum Modes" Scientific Reports 4, Article number: 4814 (2014).

[8] Pu, M., Li, X., Ma, X., Wang, Y., Zhao, Z., Wang, C., Hu, C., Gao, P., Huang, C., Ren, H., Li, X., Qin, F., Yang, J., Gu, M., Hong, M., and Luo X., "Catenary Optics for Achromatic Generation of Perfect Optical Angular Momentum," Science Advances, 1, 9, e1500396 (2015).

[9] Bernet, S., Jesacher, A., Furhapter, S., Maurer, C., and Ritsch-Marte, M., "Quantitative Imaging of Complex Samples by Spiral Phase Contrast Microscopy" Opt Express 14, 3792–3805 (2006).

[10] Messiah, A., [Quantum Mechanics, Volume II], John Wiley & Sons, New York, 507-577 (1965).

[11] Pauli, W., "The Connection Between Spin and Statistics" Phys. Rev., Vol. 58, 716 (1940).

[12] Lanzagorta, M., [Quantum Radar], Morgan & Claypool Publishers (2012).

[13] Lloyd, S., "Enhanced Sensitivity of Photodetection via Quantum Illumination," Science 321, 1463 (2008).

[14] Tan, S.H., Erkmen, B.I., Giovannetti, V., Guha, S., Lloyd, S., Maccone, L., Pirandola, S., Shapiro, J.H., "Quantum Illumination with Gaussian States," Phys. Rev. Lett. 101, 253601 (2008).

[15] Barzanjeh, S., Guha, S., Weedbrook, C., Vitali, D., Shapiro, J.H., and Pirandola, S., "Microwave Quantum Illumination" Phys Rev Lett 114, 080503 (2015).

[16] Howland, G.A., [Compressive Sensing for Quantum Imaging] Ph.D. Dissertation, Department of Physics and Astronomy, University of Rochester, Rochester, NY, 2014 (2014).

[17] Allen, E.H., Karageorgis, M., and Riga, J.M., "Sensor Systems and Methods using Entangled Quantum Particles" United States Patent 7,767,976 (2008).

[18] Lopaeva, E.D., Ruo Berchera, I., Degiovanni, I.P., Olivares, S., Brida, G., and Genovese, M., "Experimental Realization of Quantum Illumination" Phys. Rev. Lett. 110, 153603 (2013).

[19] Smith, J.F., "Using Hyperentanglement to Enhance Resolution, Signal-to-Noise Ratio, and Measurement Time" Optical Engineering 56(3), 031210 (2017).

[20] Smith III, J.F., "Quantum Entangled Radar Theory and a Correction Method for the Effects of the Atmosphere on Entanglement" Proc. SPIE 7342, Quantum Information and Computation VII, 73420A (2009).

[21] Ndagano, B., and Forbes, A., "Entanglement Distillation by Hong-Ou-Mandel Interference with Orbital Angular Momentum States" APL Photonics 4, 016103 (2019).

[22] Mazeas, F., Traetta, M., Bentivegna, M., Kaiser, F., and Aktas, D., "High Quality Photonic Entanglement for Wavelength-Multiplexed Quantum Communication based on a Silicon Chip" Optics Express, Optical Society of America, 2016, 24 (25), pp.28731-28738 (2016).

[23] Andrews, R.W., Peterson, R.W., Purdy, T.P., Cicak, K., Simmonds, R.W., Regal, C.A., and Lehnert, K.W., "Bidirectional and Efficient Conversion between Microwave and Optical Light," Nature Phys., 10, 321 (2014).

[24] Barzanjeh, S., Abdi, M., Milburn, G.J., Tombesi, P., and Vitali D., "Reversible Optical-to-Microwave Quantum Interface" Phys. Rev. Lett. 109, 130503 (2012).

[25] Bochmann, J., Vainsencher, A., Awschalom, D.D., and Cleland, A.N., "Nanomechanical Coupling between Microwave and Optical Photons," Nature Physics 9, 712–716 (2013).

[26] Roslund, J., Medeiros de Araújo, R., Jiang, S., Fabre, C., Treps, N., "Wavelength-Multiplexed Quantum Networks with Ultrafast Frequency Combs" Nature Photonics 8, 109–112 (2014).

[27] Xia, K., "Deterministic Generation of Bright Multicolor Entanglement from Optomechanical Systems" arXiv:1507.07310v1, (2015).

[28] Cheng, G.L., Chen, A.X., Zhong, W.X., "Entanglement of tripartite microwave radiation via quantum coherence in single molecular magnets" Journal of the Optical Society of America B Vol. 29, 6, 1376-1382, (2012).

[29] Stav, T., Faerman, A., Maguid, E., Oren, D., Kleiner, V., Hasman, E., and Segev, M., "Quantum Entanglement of the Spin and Orbital Angular Momentum of Photons using Metamaterials" Science, 361, 6407, 1101-1104 (2018).

[30] Ren, H., Li, X., Zhang, Q., and Gu, M., "On-Chip Noninterference Angular Momentum Multiplexing of Broadband Light" Science, 352, 6287, 805-809 (2016).

[31] Stellinga, D., Pietrzyk, M.E., Glackin, J.M., Wang, Y., Bansal, A.K., Turnbull, G.A., Dholakia, K.D., Samuel, I.D., and Krauss, T.F., "An Organic Vortex Laser" ACS Nano, 12 (3), 2389–2394 (2018).

[32] Lanzagorta, M., Jitrik, O., Uhlmann, J., Venegas, S., "Clutter Attenuation using the Doppler Effect in Standoff Electromagnetic Quantum Sensing" Proc. SPIE 9829, Radar Sensor Technology XX, 98291E (2016).

[33] Jack, B., Leach, J., Romero, J., Franke-Arnold, S., Ritsch-Marte, M., Barnett, S.M., and Padgett, M.J., "Holographic Ghost Imaging and the Violation of a Bell Inequality" Phys. Rev. Lett. 103, 083602 (2009).

[34] Lin, M., Gao, Y., Liu, P., and Liu, J., "Improved OAM-Based Radar Targets Detection Using Uniform Concentric Circular Arrays" International Journal of Antennas and Propagation, Volume 2016, Article ID 1852659 (2016).

[35] Wang, X., Song, Y., "Transmission Characteristics of Bessel–Gaussian Vortex Beams Propagating Along Both Longitudinal and Transverse Directions in A Subway Tunnel," Optical Engineering 57(2), 024105, (2018)